Title

Enhanced stimulated raman scattering of solvent due to anharmonic energy transfer from resonance raman solute molecules.

Journal

Optics Express, 28(15)

ISSN

1094-4087

Authors

Shi, Lingyan
Gayen, Taposh
Budansky, Yury
et al.

Publication Date

2020-07-20

DOI

10.1364/oe.395406

Peer reviewed

Research Article | Vol. 28, No. 15 / 20 July 2020 / Optics Express 21792
Optics EXPRESS

Enhanced stimulated raman scattering of solvent due to anharmonic energy transfer from resonance raman solute molecules

LINGYAN SHI,[1,5,*] TAPOSH GAYEN,[2,5] YURY BUDANSKY,[2] KERR YOO,[2] JEFF SECOR,[2] THOMAS HARVEY,[3] GEORGE HARVEY,[3] PAVEL SHUMYATSKY,[2] DANIEL NOLAN,[4] AND ROBERT ALFANO[2]

[1]*Department of Bioengineering, University of California San Diego, La Jolla, CA 92093, USA*
[2]*Institute of Ultrafast Spectroscopy and Lasers, the City College of New York, NY 10031, USA*
[3]*Dartmouth College, Hanover, NH 03755, USA*
[4]*Corning Inc., One Riverfront Plaza, Corning, NY 14831, USA*
[5]*Lingyan Shi and Taposh Gayen contributed equally*
[*]*Lingyanshi@ucsd.edu*

Abstract: A new nonlinear optical process, named enhanced stimulated Raman scattering (ESRS), is reported for the first time from resonance Raman in β-carotene-methanol solution. It is well known that absorption decreases the efficiency of the nonlinear optical and laser processes; however, we observed enhanced stimulated Raman peaks at the first and second Stokes from methanol solvent at 2834 cm^{-1} with the addition of β-carotene solutes. This enhanced SRS effect in methanol is attributed to the resonance Raman (RR) process in β-carotene, which creates a significant number of vibrations from RR and the excess vibrations are transferred to methanol from anharmonic vibrational interactions between the β-carotene solutes and the methanol solvent, and consequently leads to the increased Raman gain.

1. Introduction

Raman scattering is one of the well-known key optical spectroscopic processes arising from inelastic scattering of light by vibrations in materials. The Raman effect has been an active topic in various fields of science since its discovery in 1928 by Raman and Krishnan [1]. There are several different types of Raman processes that can occur, depending on the types of interactions between the laser beam and matter, such as spontaneous Raman (sR), resonance Raman (RR), stimulated Raman scattering (SRS), and surface enhanced Raman scattering (SERS). Spontaneous Raman, despite being the weakest form of scattering, has been widely used as a powerful technique to investigate complex molecular, gaseous and condensed matter systems [2]. An enhancement of the Raman signal is important for detecting low concentrations or low cross-section compounds, and this can be achieved by resonance Raman spectroscopy (RRS) when the laser excitation wavelength matches the energy of any electronic transition of a system. In RRS, the Raman intensity is proportional to the absorption coefficient $\alpha(\omega)$ for the laser wavelength in the absorption wavelength range. The signal increases from the poles of $\alpha(\omega)$ as $Ir \sim (\omega_s{}^4/\omega_L)\alpha(\omega_L)(n_o+1)I_L$, where n_o is the vibration population number for the Stokes signal and I_L is laser intensity. In the past Kaiser [3,4] and Alfano [5,6] used picosecond (ps) laser pulses in stimulated Raman Scattering (SRS) to generate excess vibrational amplitude phonons (Qs) in liquids and solids and measured the lifetimes of Q. Now we show RR can produce significant amount of Qs.

Nonlinear optical processes are usually reduced by losses in absorptions. Bloembergen [7] reviewed the early experimental and theoretical developments in his classic work on SRS. The SRS phenomenon can occur when Stokes photons are generated and accumulated in the forward

#395406 https://doi.org/10.1364/OE.395406
Journal © 2020 Received 21 Apr 2020; accepted 15 Jun 2020; published 8 Jul 2020

Optics EXPRESS

and backward directions with high intensity pump lasers. SRS was first discovered when a cell with nitrobenzene was introduced inside a ruby laser cavity [8], where a rather strong emission at the wavelength other than the pump laser wavelength was observed. Stoicheff's group measured various regimes for Raman processes at different pump laser intensities from the spontaneous Raman effect to SRS effect for the first Raman Stokes line in nitrogen and oxygen liquids. The regions are noted as spR, small SRS gain, SRS, and SRS saturation, as the pump laser intensity was increased from milliwatt to megawatt [9,10]. Several researchers have demonstrated different Raman gains from transient to steady state depending on the pulse duration and vibrational lifetime under picosecond (ps) pulses [11,12]. Kwok and Chang [13,14] observed stimulated resonance Raman scattering in micro-droplets of Rhodamine (at 10^{-3} M) collected at a larger scattering angle of 90 degrees. In SRS microscopy, the sample is coherently driven by two lasers: the pump beam with frequency ω_L and the Stokes beam with frequency ω_s, where their frequency difference is equal to a particular's Raman-active molecular vibration in the sample. The SRS signals, including both stimulated Raman loss (SRL) at the laser pump beam and stimulated Raman gain (SRG) at the Stokes beam, can be generated for imaging due to nonlinear interaction between photons and the vibration of molecules [9–12]. Current SRS microscopy was first developed by Xie group for imaging biological organisms by probing vibrations of lipids, proteins, as well as other molecules [15–17]. SRS microscopy has ever since been extensively employed for imaging metabolic dynamics of lipids, protein, glucose, nucleic acids and more in cells, tissues, and animals, both in vitro and in vivo, under physiological and pathological conditions [18–23]. The development of novel nonlinear vibrational spectroscopy has enabled broadband SRS to provide a high-intensity coherent signal with a low fluorescence background. In SRL, the sample is interrogated by a pair of overlapped narrowband ps Raman pulses and tunable broadband ps probe pulses generated by an OPO. In the SRS G/L process, the vibrational spectrum of lipids and proteins, for example, occurs with an incoherent fluorescence background, and the electronic susceptibility is efficiently suppressed. There is a need to develop methods to increase the signal-to-noise (S/N) ratio of a stimulated Raman microscope, which has been overlooked. This is partly addressed by higher frequency modulation in the MHz range that reduces the 1/f noise and the dark current.

We report for the first time the observation of a new nonlinear optical phenomenon using both electronic and vibrational state resonances for the enhancement of SRS, called enhanced stimulated Raman scattering (ESRS). This phenomenon combines RRS, energy vibration transfer between the solute and solvent molecules, and SRS nonlinear process in β-carotene-methanol solution. Absorption usually decreases the efficiency of nonlinear phenomenon, however, here we observe an enhancement of the SRS process in the solvent.

In ESRS, the electronic response vibrational resonance occurs in the carotene solute via RRS followed by energy vibrational interaction between the solvent and solute. The RR can create a significant number of vibrations of Q, such as in the SRS process [24–26]. In this manner, the Raman signals are increased with the carotene concentration. This increase in solvent with additional absorption is unusual. The observed effect of the ESRS in small signal gain is attributed to the fact that the RR process in carotene creates significant amount of additional vibrational Q which are transferred to methanol from anharmonic vibrational interactions between the carotene solute in resonance with the vibration of the methanol solvent. The observation of ESRS is significantly different from Kwok and Chang's study [13,14] despite the similarity of the name resonance stimulated Raman scattering (RSRS). The gain in ESRS arises in the solvent methanol is due to resonance energy transfer from resonance Raman process in solute carotenes in a well defined beam following the pump laser beam direction.

Optics EXPRESS

2. Experimental results

To understand the observed ESRS process, we examined the relationship between the absorbance of β-carotene in methanol, the wavelength, and the enhancement of the Raman scattering by resonance, using a Cary 500 UV-VIS NIR spectrophotometer. The absorbance increases with increasing β-carotene concentration, reaching a peak at approximately 450 nm and with the absorbance tail extending to 550 nm. Using the absorption tail wavelength of 532 nm as the pump laser wavelength in an Ocean Optics Raman microscope, we carried out spontaneous Raman on methanol and on β-carotene in methanol to identify their salient peaks, as shown in Fig. 1.

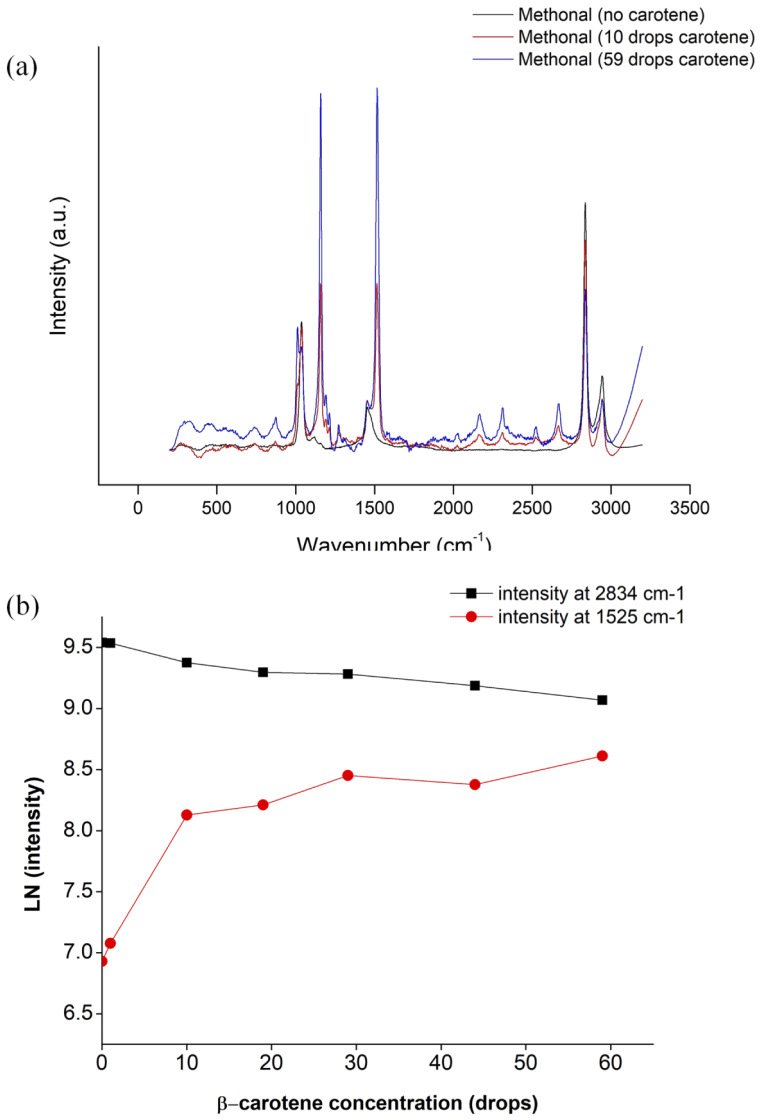

Fig. 1. Resonance Raman intensity at different concentrations of β-carotene. (a) Resonance Raman spectra for methanol solution containing different concentrations (drops) of β-carotene. The carotene vibrations at 1152 cm^{-1} and 1525 cm^{-1} are resonance modes. (b) The relationship between the Raman peak intensity (1525 cm^{-1} and 2834 cm^{-1}) and β-carotene concentration. The intensity is plotted on a natural log scale. The intensity at 1525 cm^{-1} (red) increases approximately 4-fold and the intensity at 2834 cm^{-1} (black) decreases slightly with increasing β-carotene concentration (up to 59 drops of carotene).

Optics EXPRESS

When there was no β-carotene in methanol (black line, Fig. 1(a)), the most significant Raman peak for methanol appeared at 2834 cm^{-1}, with minor peaks located at 1035 cm^{-1} and 1425 cm^{-1}. The Raman peaks of the β-carotene solution occurred at 1525 cm^{-1}, 1157 cm^{-1} and 2834 cm^{-1}. With a low concentration of β-carotene (10 drops, red line, Fig. 1(a)) in methanol, the peak intensities at 1525 cm^{-1} and 1157 cm^{-1} increased, while the peak at approximately 2834 cm^{-1} slightly decreased; with a high concentration of β-carotene (59 drops, blue line, Fig. 1(a)), the peaks at 1525 cm^{-1} and 1157 cm^{-1} further increased, while the peak at 2834 cm^{-1} further decreased.

Figure 1(b) shows the relationship between the intensity of the Raman peaks and β-carotene concentrations at 1525 cm^{-1} and 2834 cm^{-1}. The intensities of the peaks at 1525 cm^{-1} increased with the concentration of β-carotene in methanol, and consequently, the absorption (also called optical density, OD) of the solution increased. We found that the intensity of the β-carotene's Raman peaks were enhanced by resonance Raman effects, as observed in the Raman spectra. The peak intensity at 2834 cm^{-1} decreased when the absorption of the solution increased as a result of adding more β-carotene into the solution; however, the intensity did not fall as rapidly as one would have predicted by the exponential Beer-Lambert law, instead, it decreased algebraically. This phenomena suggested that certain interactions between methanol solvent molecules and β-carotene molecules led to a slightly increase at 2834 cm^{-1} mode following the addition of β-carotene into the solution. The 1525 cm^{-1} and 1157 cm^{-1} modes from carotene and from the methanol or carotene bath can provide the vibrations to produce more modes at 2834 cm^{-1} from methanol over the thermal background.

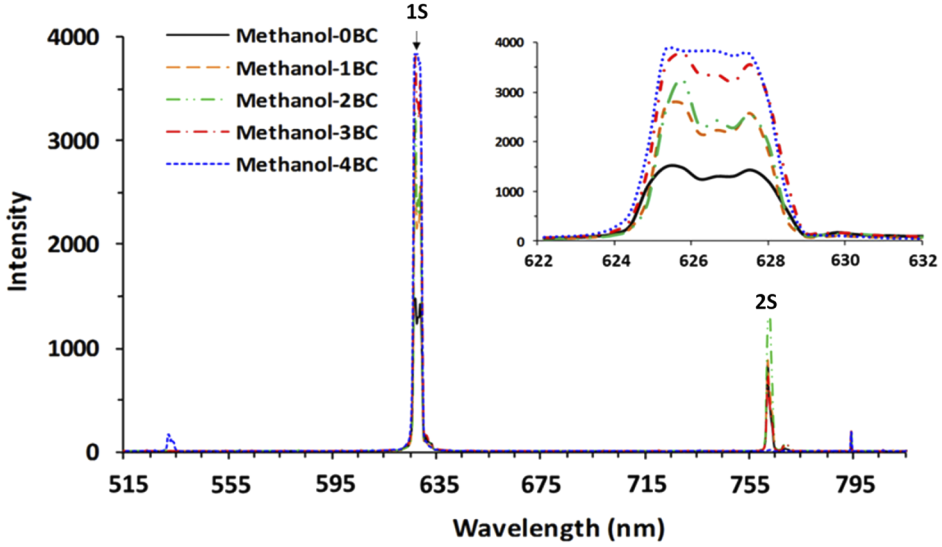

Fig. 2. Effects of enhanced resonance stimulated Raman scattering (ESRS) as a function of wavelength. The primary peak (1S) and secondary peak (2S) are marked by increasing concentrations of β-carotene in methanol solution when excited by a high-power pulsed laser beam. "0BC" denotes no β-carotene, and the β-carotene concentration increases from "1BC" to "4BC". The inset in the upper right corner shows the intensities in the amplified wavelength region 622–632 nm. Saturation is noted at 1S band in the inset.

ESRS experiment of β-carotene in methanol was carried out using a Q-switched Quanta Ray Nd:glass laser with a pumping wavelength of 532 nm. The measured ESRS spectra of β-carotene in methanol at different concentrations are shown in Fig. 2. As the concentration of β-carotene was increased, the signal intensity from the first Stokes line (1S) of methanol at 626 nm increased, and the second Stokes line (2S) of methanol appeared at ~762 nm. A bright red beam appeared on a white card when we looked through a 3-67 filter at the output of the

Optics EXPRESS

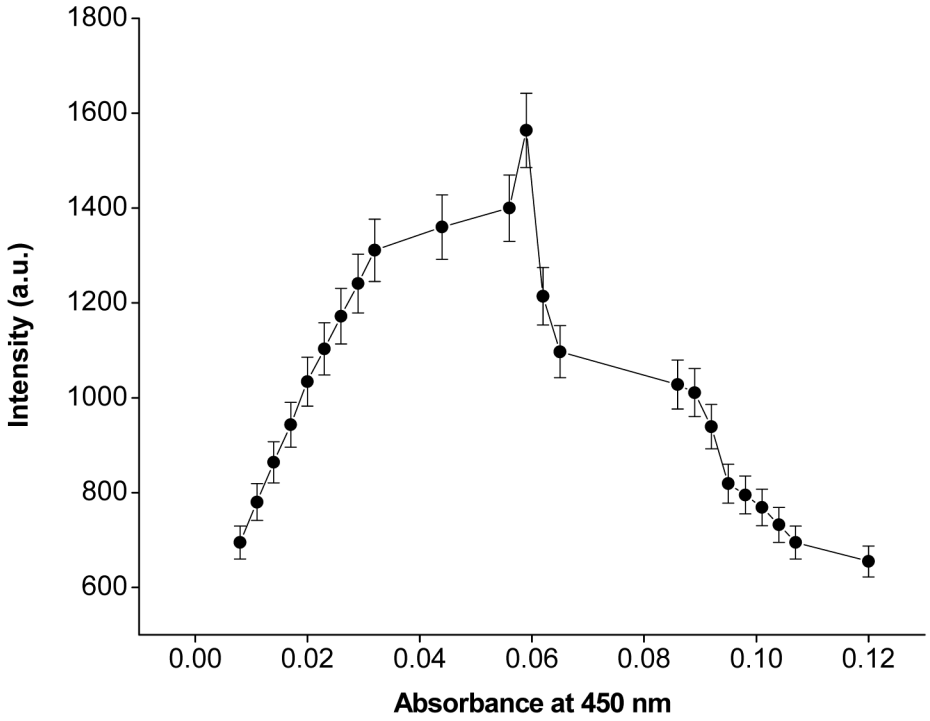

Fig. 3. SRS profile for the 1S Raman intensity versus absorption (OD). This plot shows how the first-order (1S) resonance peak intensity increases with absorption at 450 nm for β-carotene in methanol solution. The SRS signal increases with increasing absorption up to a certain limit (i.e., 0.06) due to the ESRS mechanism.

cell. The red beam became stronger when we added more drops of carotene into the methanol. The Raman effects were transferred to the CH_3 vibrational mode of methanol at 2834 cm^{-1} from carotene's lower frequencies. No SRS beam was observed for carotene at 1528 cm^{-1} or 1152 cm^{-1}. This phenomenon was likely caused by energy transfer from carotene solute to the surrounding methanol host solvent. We also observed that SRS signal grew with higher carotene concentrations at the same 532 nm excitation laser.

Figure 3 shows 1S Raman signal vs. absorbance of OD of carotene. The salient feature of this ESRS study shows that the SRS first Stokes (1S) signal at 626 nm initially increases linearly with the absorption of carotene. The RR from the carotene is the source of the extra excited Q for methanol above the thermal vibration background n_T. At an absorbance of 0.03, the signal flattens, most likely due to generation of a second Stokes signal (2S); beyond an absorbance of 0.06, the SRS signal decreases due to excessive absorption. The ESRS beam profile at 626 nm follows the 532 nm pump beam path as measured on a card. The addition of carotene absorption demonstrates that the SRS intensity is enhanced due to resonance behavior, which generates ESRS effects at 1S, leads to the appearance of the 2S for methanol at higher absorbance (as shown in Fig. 1), and increases the intensity for the 2834 cm^{-1} mode. The observation of ESRS is important, as it has potential for applications in new versions of SRS microscopes for imaging vibrations from samples using ESRS loss and gain mechanisms. RR from a solute can act as a source of vibrations for the solvent.

Optics EXPRESS

3. Empirical model on SRS and RR enhancement

3.1. SRS and resonance Raman background

The intensity for spontaneous Raman (sR) is weak (10^{-6} I_L) [2,24], where I_L is the laser intensity. The scattered power is given by

$$P_s = N\left(\frac{\partial\sigma}{\partial\Omega}\right)_R \Delta\Omega\, I_L = N\sigma_R I_L \propto (\omega_S{}^4/\omega_L)\alpha(\omega_L)(no+1)I_L \tag{1}$$

where the cross-section is given by:

$$\sigma_R = \left(\frac{\partial\sigma}{\partial\Omega}\right)_R d\Omega \tag{2}$$

N is the number of molecules in the observed volume, $\left(\frac{\partial\sigma}{\partial\Omega}\right)$ is the differential Raman cross-section and $\alpha(\omega_L)$ is the absorption coefficient.

When the excitation laser wavelength approaches an electronic absorption in a material, the transitions among states transform from virtual to real. The Raman scattering signal becomes enhanced due to the resonance effect. The enhancement in the cross section arises from the energy denominator in the nonlinear susceptibility (see Eqs. (3) and (4)), becoming small as the laser frequency matches the electronic energy states. The virtual transition for the intermediate state becomes real and the Raman effect becomes 10- to 1000-fold larger depending on how close the laser photon energy is to the transition energy from the ground state (i) to the electronic state (j). The Raman intensity increases when either the in resonance or out resonance for the electronic states occur with the pump and Raman shifted light. This process is called resonance Raman scattering (RRS) [2,24–26].

The Raman cross-section for a single molecule from electronic resonances is given by:

$$\sigma_R = \left|\sum \frac{A_{ijjf}}{(\omega_{ij} - \omega_L - i\Gamma_j)} + \frac{A_{jijf}}{(\omega_{jf} - \omega_q - i\Gamma_j)}\right|^2 \tag{3}$$

where the poles are $\omega_{ij} = \omega_L$ and $\omega_{jf} = \omega_q$ for in and out resonances plus 5 other terms. In addition, the resonance vibrations occur at Stokes and laser where $\delta(\omega_S + \omega_q - \omega_L)$ is the vibrational response of the Raman process and the $\omega_{\text{Stokes}} = \omega_L - \omega_q$. When ω_L approaches ω_{ij}, the denominator reduces and σ_R increases, thus, Raman becomes RRS. The frequency dependence of the cross section in Eq. (3) shows the salient resonance features between the pump and probe frequency and the electronic absorption for enhancement.

The quantum mechanical description for the resonance Raman term, R, from Fermi's Golden Rule via Loudon [26] is:

$$R_{12} = \left(\sum{}_{\alpha,\beta} \frac{P_{0\alpha}E_{\beta\alpha}P_{\alpha 0}}{(\omega_\beta + \omega_0 - \omega_L)(\omega_\alpha - \omega_L)} + 5\text{ terms}\right) \tag{4}$$

where P is the dipole moment and E is the deformation potential in the Hamiltonian, ω_L = laser, ω_0 = phonon, and α, β are electronic states. The poles are at $\omega_\beta = \omega_L - \omega_0$ and $\omega_\alpha = \omega_L$, which give rise to a resonant Raman effect. The Raman scattering efficiency is proportional to $(no+1)$ for the Stokes signal and no for the anti-Stokes signal where no is the vibration population factor [24–26].

When an intense laser pulse (such as ns, ps, and fs) enters a material, the Raman effect occurs. The light is first scattered over a large angle Ω. As the Raman light travels with the pump laser in the forward and backward directions, it can become larger than the Raman light traveling out of the beam at other angles, as it propagates together with the laser pulse over a length of more than

Optics EXPRESS

10 cm. Depending upon the intensity of the laser pump pulse, the Raman light in the forward and backward directions may become so large that it can be stimulated and become laser–like with high direction and coherence.

The intensity of the Raman Stokes gain in SRS is given by a Beer-Lambert law-like equation [2,7,24,26]:

$$I_{RS}(z) = I_{RS}(0)\exp(Gz - \alpha z) \tag{5}$$

where G is the gain, α is the loss, and $I_{RS}(0)$ is the initial Stokes signal from zero point fluctuation, which shows SR at z = 0.

The Raman gain G is given as

$$G = N\left(\frac{\partial\sigma}{\partial\Omega}\right) I_L \Delta\Omega \tag{6}$$

In any SRS, the Raman gain must exceed the loss due to absorption in the media [5], where Gz > 25; in addition, the medium will experience an exponential growth of photons at the Stokes frequency. The Raman light in the forward direction becomes much greater than spontaneous Raman and becomes SRS with approximately 1% to 10% of the energy transferred from the pump frequency. For small SRS gain, Eq. (5) reduces to:

$$\mathrm{I_{RSR}} = \mathrm{I_{RS}}\,(1 - \mathrm{Gz}) \tag{7}$$

and the SRS signal difference is given by

$$\Delta\mathrm{I_{SRS}} = \mathrm{AI_{RS}I_L z} \tag{8}$$

where A is a constant. There is loss at the pump and gain at the Stokes in SRS. In this region Eq. (8) is the base of the SRS L/G microscope.

3.2. Empirical model of ESRS gain effect from RR of solute to solvent

The observation of Raman gains in Fig. 3 at 2834 $\mathrm{cm^{-1}}$ vibration mode for a binary solution of solvent (methanol, M) with solute (carotene, C) is attributed to the RR of solute C with vibrational energy transferred from C to excite M vibrations via anharmonic interactions, as depicted in Fig. 4.

The following gives an empirical model that explains the gain to solutes from anharmonic effect [27,28]. We extend Kaiser's pioneering research [29,30] on energy transfer and decay of vibrations in mixed liquids for the generation of an excess of excited vibrations by RR process and energy transfer from C to M. In support of the proposed model, an order of magnitude calculation follows to explain the observed Raman small gain of M from an excess of M vibration with increasing C concentration, which in turn leads to more excited M from C molecules via the RR effect of C molecules.

The magnitude of the sR intensity is approximately given by:

$$\mathrm{I_{sR}} = 10^{-6}\mathrm{I_L} \tag{9}$$

and the RR intensity is increased by about >1000 fold, given by

$$I_{RR} \sim 10^{-3} I_L \text{ to } 10^{-2} I_L \propto (\omega_S{}^4/\omega_L)\,\alpha(\omega_L) I_L \tag{10}$$

where the Stokes signal is ~ ($\mathrm{n_o}$+1), where $\mathrm{n_o}$ is the population number of vibrations for the Stokes photons.

Optics EXPRESS

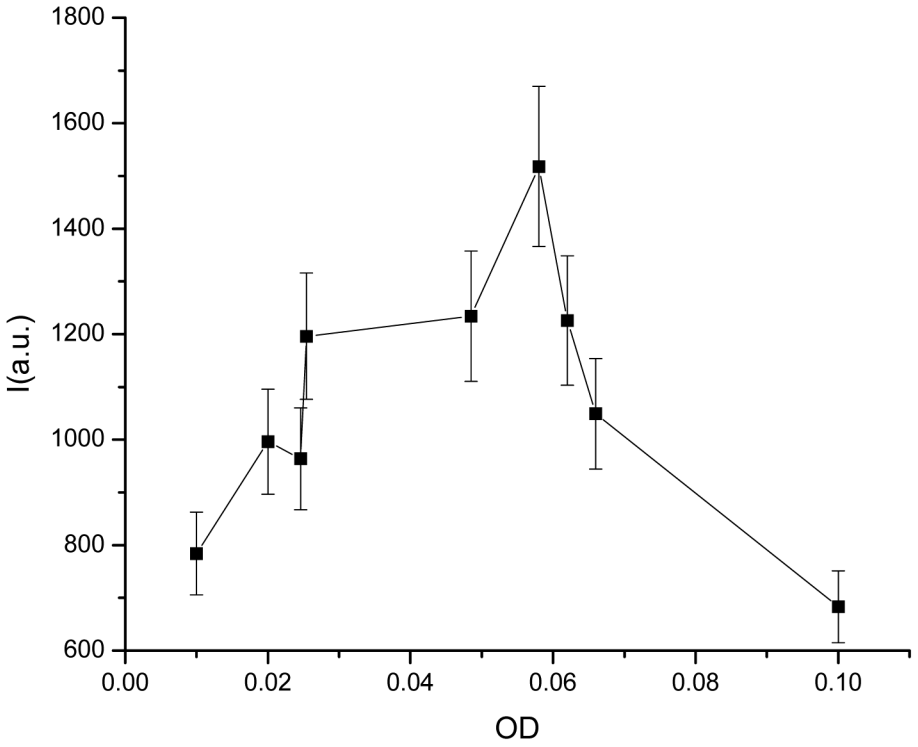

Fig. 4. ESRS of 2924 cm^{-1} from acetone vibrational modes. Acetone +β-carotene, OD = 0.1.

The excess vibrations generated by the RR process are similar in number to that created by SRS. The number of photons for the pump laser at 5 mJ of 5 ns duration at 532 nm is

$$N_L \sim 1.46\, x\, 10^{16} \text{photons} \tag{11}$$

The number of carotene vibrational modes (nc) created via Resonance Raman is about $\sim 10^{-3}$-fold smaller:

$$nc = (10^{-3})\,(1.46 \times 10^{16}) = 1.46 \times 10^{13} \text{ vibrations} \tag{12}$$

The excitation laser volume V calculated from the beam diameter of approximately 100 µm and length of approximately 2 cm is:

$$V = 2 \times 10^{-4} cm^3 \tag{13}$$

Thus, the number of excited vibrations per cm^3 from RR is:

$$nc = (1.46 \times 10^{13}) / (2 \times 10^{-4}) = 0.73 \times 10^{17} \text{ vibrations / } cm^3 \tag{14}$$

The number of molecules per volume of a liquid is approximately $5 \times 10^{21}/cm^3$. The total number of excited carotene molecules for a 10^{-4} molar solution gives the number of carotene molecules:

$$Nc = (5 \times 10^{21})(10^{-4}) = 5 \times 10^{17} \text{carotene molecules}/cm^3 \tag{15}$$

The occupation number of carotene vibrations in excess of the thermal number at the frequency of 1152 cm^{-1} and 1525 cm^{-1} is about :

$$\text{nc (C vibration)} = \text{Nc vibrations/ Nc molecules} = (0.73 \times 10^{17}/cm^3) / (5 \times 10^{17}/cm^3)$$
$$nc = 1.46 \times 10^{-1} \tag{16}$$

Optics EXPRESS

which is larger than the thermal occupation numbers of

$$n_T = 10^{-6} \text{for } 3000\ \text{cm}^{-1} \text{modes and } n_T = 10^{-2} \text{for } 1000\ \text{cm}^{-1} \text{modes} \tag{17}$$

The vibrational energy transfer of carotene vibrations with an efficiency of $\eta = 10^{-2}$ from carotene to methanol gives the occupation number for methanol vibrations:

$$n_0(\text{methanol}) = 1.46 \times 10^{-3} \tag{18}$$

which is still greater than the thermal occupations for $3000\,\text{cm}^{-1}$ modes. Even if a lower value of $\eta = 10^{-4}$ is used, the n_0 of excess methanol vibrations is $> n_T$.

The vibration excitation of methanol via RR of carotene over the thermal occupation mode at $3000\,\text{cm}^{-1}$ is

$$n_0 / n_T = 1.46 \times 10^{-3} / 10^{-6} = 1.46 \times 10^{3} \tag{19}$$

which is 1.46×10^3 times greater than the thermal effect due to hot M vibrations.

This model describes the build–up energy for methanol from RR of carotene vibrational modes. The rate equation is governing the population of methanol vibrations n_M due to energy transfer from carotene n_C* to methanol with a transfer efficiency of η given by:

$$dn_M / dt = - n_M / T_1 + \eta\, n_C^* / T_0 \tag{20}$$

where T_1 is the depopulation relaxation time for M and T_0 is the repopulation relaxation time of excited RR carotene. The first term represents the decay in the methanol occupation vibration n_M, and the second term represents the feeding of M. The steady-state occupation for methanol is given by

$$n_M = \eta n_C^*\, T_1 / T_0 \tag{21}$$

The RR enhanced small signal gain of methanol, from Eq. (8), becomes:

$$\Delta I_{SRSR} \approx g I_L I_S z = n_M \sigma I_L I_S\, z \tag{22}$$

The cross-section gives the enhancement of the ESRS signal via RR.

4. Methods

The β-Carotene powder was dissolved into methanol as stock solution, and was then added gradually into a 20 cm optical glass cell containing methanol solution. Following capture of the intensity profile for the 20-cm cell under laser illumination, 1-cm glass cells were used to collect the solution and measure the optical density of the dissolved carotene in methanol.

The experimental setup consists of a Cary 500 UV-VIS NIR spectrophotometer used for measuring the absorbance, and an Ocean Optics 1D Micro Raman microscope used to capture the resonance Raman (not shown here) spectra. For ESRS experiments, a Q-switched Quanta Ray Nd:glass laser equipped with a 1064 nm laser beam and SHG KPD crystal provided a laser excitation beam at 532 nm. The excitation power was set to produce approximately 5 mJ per pulse at a pulse duration of 5 ns. A 20-cm glass cell tube was used to hold methanol solution containing β-carotene for the SRS experiments. A converging lens with a focal length of 30 cm was used to focus the laser beam onto the cell. One 1-75 filter was used to block the 1064 nm laser light before the laser beam impinged upon the cell holding the methanol solution, and two 3-67 color filters were used in front of the spectrometer to block any trace of the 532 nm laser beam. An Ocean Optics spectrometer was used to detect the stimulated Raman (SR) spectra. Neutral-density filters were used to adjust the SRS signal at the input to the spectrometer to avoid SRS signal saturation arising from the interaction of the pump beam with the β-carotene methanol solution.

Optics EXPRESS

5. Additional support to ESRS process for carotene and acetone

We used acetone to test another solvent for ESRS. The ERRS in Acetone +β-Carotene, using Q-Switch 532 nm laser and 20 cm cell was observed in Fig. 4.

6. Discussion

In this research, we showed that β-carotene provides the methanol with enhancement of the Raman cross-section in the visible region where its absorption peaks at 450 nm and the absorption tail extends beyond 532 nm. The main absorption for carotene is from the 2S state, as the 1S state is dipole forbidden**.** The concentration of carotene was varied from adding a stock 10^{-4} M solution by drops into methanol liquid. And a red (626 nm) SRS beam from methanol was observed when the carotene stocks were added into a 20 cm long optical glass cell. We used empirical model to describe this ESRS process of solvent methanol (and acetone) from RR interactions with solute (carotene).

The salient features of the ESRS observations include: 1) SRS signal increased at methanol's vibrational frequencies due to the presence of carotene; 2) carotene's absorption was from the 2S state, with little fluorescence; 3) carotene and methanol became a coupled material, with SRS occurred from the methanol CH_3 bond but not at a carotene vibrational mode; and 4) resonance Raman occurred when the laser wavelength fell in the absorption wing for in resonance of carotene, or fell the peak emission for out resonance of carotene.

The salient observation of this study is that the carotene solute's RRS enhanced SRS signal from the vibrations of methanol. The solute-solvent system can have different types of interactions: vibrations between solute-solute molecules, solvent-solvent molecules, or solute-solvent molecules [27–30]. The spontaneous Raman signal at 2834 cm^{-1} (Fig. 1(a)) was a coupling effect. The mechanism for the ESRS from solute to solvent was due to the anharmonic coupling between solute and solvent. The anharmonic coupling allows the flow of energy among vibrational modes. A cubic anharmonicity enables exchange of the excitation of the solute and solvent vibration modes during interactions.

Vibrational energy processes in a binary solvent A and solute B system can have cubic and quartic interactions [29,30]. A possible interaction in methanol solvent from the resonance Raman of carotene is the generation and deactivation of 2834 cm^{-1} and 152 cm^{-1} methanol bath phonons, respectively, by the 1525 cm^{-1} and 1157 cm^{-1} modes, for instance, 1525 cm^{-1}+ 1157 cm^{-1} → 2834 cm^{-1}1−152 cm^{-1}. Figure 5 shows a schematic energy diagram for the potential quartic vibrations attributed to the enhancement of SRS at the 2834 cm^{-1} mode involved in the resonance Raman of carotene. As shown in Fig. 5, upon excitation at 532 nm, carotene undergoes RR scattering at 1525 cm^{-1} and 1157 cm^{-1}, and then transfers energy to methanol, with bath phonons at 152 cm^{-1} from methanol, exciting the methanol mode at 2834 cm^{-1}. The data shown in Fig. 1 for RR supports the energy transfer model from carotene to methanol at 2834 cm^{-1}.

In the past, Kaiser's group investigated cubic interactions, i.e., one excited molecule, say A*, decays though resonant and non-resonant interaction in cubic collisions: A*AA, A*AB, and A*BB. Such cubic interactions can affect the decay lifetime of the vibration [29,30]. They observed the cubic interaction of higher vibration CH_3 (A) following addition of CCl_4 liquid (B). The vibrational lifetime for the A* of CH_3 increases with the concentration of B. Therefore, the Raman gain increased following the addition of CCl_4 with a crossover from transient gain to steady-state gain. Raman gain increases more towards steady-state when the lifetime of the vibrations increases. This effect is more important when one uses femtosecond and picosecond pulses laser but not a nanosecond pump laser. Therefore, in this study, the resonance of B (i.e., carotene) to A (i.e., methanol) was the major contributor to the ESRS process.

The solute carotene affects the transfer of vibrations (1525 cm^{-1} + 1152 cm^{-1}) of the resonance to the solvent methanol (M) (2834 cm^{-1} and phonon bath at 152 cm^{-1}) in a quartic interaction,

Optics EXPRESS

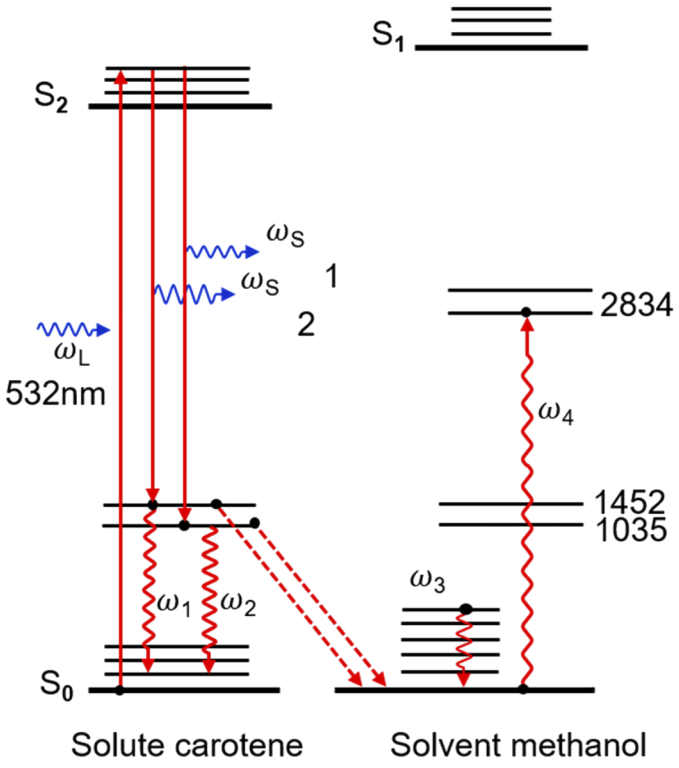

Fig. 5. Schematic for the vibrational modes of carotene and methanol. Arrows indicate transitions for cubic and quartic interactions. There is an energy transfer involving vibrational states from the carotene solute to the surrounding methanol solvent, as shown by the dash lines and wavy lines. $\omega 1 = 1525\,\mathrm{cm}^{-1}$, $\omega 2 = 1157\mathrm{cm}^{-1}$, $\omega 3 = 152\,\mathrm{cm}^{-1}$, $\omega 4 = 2834\,\mathrm{cm}^{-1}$, and $\omega 4 = \omega 1 + \omega 2 + \omega 3$, where $\omega 3$ is solvent thermal bath molecule.

$\omega_1 + \omega_2 + \omega_3 = \omega_4$, thereby enhancing the cross section. A theoretical analysis following [24–26] on the underlying physics is needed to explain the ESRS process observed from the vibrations of the carotene solute and methanol solvent.

In the future, a time-resolved femtosecond pump-probe spectroscopy can be used to test the speculative mechanism and empirical model for energy transfer presented here for ESRS. The discovery of ESRS can be important for improving SRS microscopy signals for biomedical optical imaging. To implement the observed effect in an ESRS microscope, the pump laser needs to excite at tail region of molecules' absorption spectrum or the beginning region of the emission spectrum. For example, 532 nm excitation wavelength is located in the tail of the flavins' absorption spectrum in tissues and cells, therefore, a tunable laser in the wavelength range from 570 to 650 nm can be used to increase the SR gain for either CH_2 bonds ($2850\ \mathrm{cm}^{-1}$) of lipids, or CH_3 bonds ($2930\ \mathrm{cm}^{-1}$) of proteins. It can be other chemical bonds in different biomolecules in biological tissues and cells, too.

ESRS combines both RRS and SRS processes for a new nonlinear optical (NLO) effect. The underlying mechanism is under investigation and needs more experiments to validate it. The observation of ESRS is still very important for new SRL and SRG microscopes to enhance signals of biomolecules in biological tissues, cells, or even other chemical samples. Our experiment of carotene in acetone also demonstrated a smaller ESRS gain effect due to larger vibrational mismatch ($253\ \mathrm{cm}^{-1}$ for acetone in comparison with $156\ \mathrm{cm}^{-1}$ for methanol at ω_3 mode) from anharmonic interactions: $\omega_4 = \omega_1 + \omega_2 + \omega_3$. Thus a careful and appropriate selection for the

Optics EXPRESS

pump or Stokes signal near the electronic resonance region will improve the signal to noise ratio (S/N) of the SRS microscope image.

Funding

University of California, San Diego (Startup funding); National Institutes of Health (U54 pilot grant CA132378 and 2U54CA132378-11A1); Corning Incorporated Foundation (71198-0013); Army Research Office (W911NF19110373).

Acknowledgments

We thank Luyao Lu for discussion.

Disclosures

The authors declare no conflicts of interest.

References

1. C. V. Raman and K. Krishnan, "A new type of secondary radiation," Nature **121**(3048), 501–502 (1928).
2. G. New, *Introduction to Nonlinear Optics* (Cambridge Press, 2011), pp. 87–89, pp. 186-188.
3. D. von der Linde, A. Laubereau, and W. Kaiser, "Molecular vibrations in liquids: Direct measurement of the molecular dephasing time; Determination of the shape of picosecond light pulses," Phys. Rev. Lett. **26**(16), 954–957 (1971).
4. A. Laubereau, D. von der Linde, and W. Kaiser, "Direct measurement of the vibrational lifetimes of molecules in liquids," Phys. Rev. Lett. **28**(18), 1162–1165 (1972).
5. R. R. Alfano and S. L. Shapiro, "Optical phonon lifetime measured directly with picosecond pulses," Phys. Rev. Lett. **26**(20), 1247–1251 (1971).
6. R. R. Alfano and S. L. Shapiro, "Establishment of a molecular-vibration decay route in a liquid," Phys. Rev. Lett. **29**(25), 1655–1658 (1972).
7. N. Bloembergen, "The stimulated Raman effect," Am. J. Phys. **35**(11), 989–1023 (1967).
8. E. J. Woodbury and W. K. Ng, "Ruby laser operation in the near IR," Proc. IRE **50**, 2367 (1962).
9. J. B. Grun, A. K. McQuillan, and B. P. Stoicheff, "Intensity and gain measurements on the stimulated Raman emission in liquid O_2 and N_2," Phys. Rev. **180**(1), 61–68 (1969).
10. M. Sparks, "Stimulated Raman and brillouin scattering: parametric-instability explanation of anomalies," Phys. Rev. Lett. **32**(9), 450–453 (1974).
11. R. L. Carman, F. Shimizu, C. S. Wang, and N. Bloembergen, "Theory of Stokes pulse shapes in transient stimulated Raman scattering," Phys. Rev. A **2**(1), 60–72 (1970).
12. R. L. Carman, M. E. Mack, F. Shimizu, and N. Bloembergen, "Forward picosecond Stokes-pulse generation in transient stimulated Raman scattering," Phys. Rev. Lett. **23**(23), 1327–1329 (1969).
13. A. S. Kwok and R. K. Chang, "Stimulated resonance Raman scattering of Rhodamine 6G," Opt. Lett. **18**(20), 1703–1705 (1993).
14. A. S. Kwok and R. K. Chang, "Fluorescence seeding of weaker-gain Raman modes in microdroplets: enhancement of stimulated Raman scattering," Opt. Lett. **17**(18), 1262–1264 (1992).
15. C. W. Freudiger, W. Min, B. G. Saar, S. Lu, G. R. Holtom, C. He, J. C. Tsai, J. X. Kang, and X. S. Xie, "Label-free biomedical imaging with high sensitivity by stimulated Raman scattering microscopy," Science **322**(5909), 1857–1861 (2008).
16. W. Min, C. W. Freudiger, S. Lu, and X. S. Xie, "Coherent nonlinear optical imaging: Beyond fluorescence microscopy," Annu. Rev. Phys. Chem. **62**(1), 507–530 (2011).
17. C. W. Freudiger, W. Yang, G. R. Holtom, N. Peyghambarian, X. S. Xie, and K. Q. Kieu, "Stimulated Raman scattering microscopy with a robust fibre laser source," Nat. Photonics **8**(2), 153–159 (2014).
18. Y. Yu, A. S. Mutlu, H. Liu, and M. C. Wang, "High-throughput screens using photo-highlighting discover BMP signaling in mitochondrial lipid oxidation," Nat. Commun. **8**(1), 865 (2017).
19. M. Ji, M. Arbel, L. Zhang, C. W. Freudiger, S. S. Hou, D. Lin, X. Yang, B. J. Bacskai, and X. S. Xie, "Label-free imaging of amyloid plaques in Alzheimer's disease with stimulated Raman scattering microscopy,"," Sci. Adv. **4**(11), eaat7715 (2018).
20. L. Shi, C. Zheng, Y. Shen, Z. Chen, E. Silveira, L. Zhang, M. Wei, C. Liu, C. de Sena-Tomas, K. Targoff, and W. Min, "Optical imaging of metabolic dynamics in animals," Nat. Commun. **9**(1), 2995 (2018).
21. L. Shi, Y. Shen, and W. Min, "Visualizing protein synthesis in mice with in vivo labeling of deuterated amino acids using vibrational imaging," APL Photonics **3**(9), 092401 (2018).
22. Y. Shen, F. Hu, and W. Min, "Raman Imaging of Small Biomolecules," Annu. Rev. Biophys. **48**(1), 347–369 (2019).

Optics EXPRESS

23. L. Zhang, L. Shi, Y. Shen, Y. Miao, M. Wei, N. Qian, Y. Liu, and W. Min, "Spectral tracing of isotope deuterium for imaging glucose metabolism," Nat. Biomed. Eng. **3**(5), 402–413 (2019).
24. P. E. Powers and J. W. Haus, *Fundamentals of Nonlinear Optics* (CRC Press, 2011), pp. 217–221, pp. 49-54.
25. M. M. Suschinskii, *Raman Spectra of Molecules and Crystals* (Israel Program for Scientific Translations, Wiley, New York, 1972).
26. R. Loudon, "Theory of the first-order Raman effect in crystals," Proc. R. Soc. Lond. A **275**(1361), 218–232 (1963).
27. V. V. Kenkre, A. Tokmakoff, and M. D. Fayer, "Theory of vibrational relaxation of polyatomic molecules in liquids," J. Chem. Phys. **101**(12), 10618–10629 (1994).
28. P. Moore, A. Tomakoff, T. Keyes, and M. D. Fayer, "The low frequency density of states and vibrational population dynamics of polyatomic molecules in liquids," J. Chem. Phys. **103**(9), 3325–3334 (1995).
29. K. Spanner, A. Laubereau, and W. Kaiser, "Vibrational energy redistribution of polyatomic molecules in liquids after ultrashort infrared excitation," Chem. Phys. Lett. **44**(1), 88–92 (1976).
30. A. Laubereau, L. Kirschner, and W. Kaiser, "Direct observation in intermolecular transfer of vibrational energy in liquids," Opt. Commun. **9**(2), 182–185 (1973).